Application of non-stationary iterative time-domain deconvolution

ERGUN ERHAN AND ROBERT L. NOWACK

Department of Earth, Atmospheric, and Planetary Sciences, Purdue University, West Lafayette, IN 47907, USA (erhanergunjfm@gmail.com, nowack@purdue.edu)

Received: August 12, 2019; Revised: October 8, 2019; Accepted: November 20, 2019

ABSTRACT

In this study, non-stationary iterative time-domain deconvolution (CNS-ITD) is investigated. The propagating wavelets are first estimated in several overlapping Gabor windows of the data. Matrix-vector operations in the time-domain are then performed by estimating a small number of columns of the wavelet matrix by interpolation within a sparse iterative estimation for the largest reflectivities. The iteration process is stopped when a minimum root mean square (RMS) residual or a maximum number of iterations is reached. Although initially formulated on the basis of work in earthquake seismology, CNS-ITD is a matching pursuit type of approach performed continuously in the time-domain for the non-stationary case. The results can then be convolved with a higher frequency wavelet in order to make the results stationary in time and to increase the resolution of the data. We first apply CNS-ITD to synthetic data with a time-varying attenuation, where the method successfully identifies the largest reflectors in the data. We then apply CNS-ITD to two observed shallow seismic datasets where improved resolution is obtained.

Keywords: iterative deconvolution, enhanced resolution, time-series analysis

1. INTRODUCTION

Seismic deconvolution can be used to remove the effects of the seismic wavelet and increase the frequency bandwidth of the data. It is based on the assumption that the seismic trace can be described by a time-invariant convolutional model. In practice, however, seismic data are often non-stationary due to changes in the character and frequency content of seismic waves as they propagate through the subsurface. Seismic waves will lose amplitude and broaden with time from seismic attenuation and scattering effects, and are therefore often more appropriately described as a combination of time-invariant and time-variant processes.

There are several time-variant deconvolution approaches to estimate the reflectivity. To obtain the propagating wavelets at different times, the seismic trace can be divided into several overlapping windows. The propagating wavelets estimated in these windows can be used to recover the local reflectivity and compensate for the attenuation and scattering effects. The windowed segments of the seismic trace can then be blended together to

Stud. Geophys. Geod., 64 (2020), 76–99, DOI: 10.1007/s11200-019-1165-z

obtain the full reflectivity. Gabor deconvolution (*Margrave and Lamoureux, 2001, 2019*; *Margrave et al., 2005*) and time-variant spectral whitening (*Yilmaz, 2001*) have been proposed to deal with these non-stationary effects. Inverse Q filtering can be used to compensate specifically for the effects of seismic attenuation (*Kjartansson, 1979*; *Hale, 1981*; *Wang, 2006, 2008*). *Von der Baan (2012)* applied a combination of phase-only inverse Q-filtering and time-varying Wiener deconvolution. *Morozov et al. (2018)* presented an approach for time-varying deconvolution using iterative time-domain deconvolution. Their approach is based on forward modeling of the seismic wavelet that can be estimated from the early arrivals of the seismic trace using the knowledge of a Q model and iteratively removing the modeled seismic wavelet from the seismic trace assuming that the propagating wavelet is not changing within short time windows.

Using Gabor deconvolution based on a non-stationary convolutional model, deconvolution and inverse Q filtering can be combined without requiring explicit knowledge of Q in a data-driven frequency-domain approach (*Margrave, 1998*). Similar to other frequency-domain deconvolution approaches, Gabor deconvolution can amplify the high-frequency noise in the seismic data. It also assumes a stationary propagating seismic wavelet over the individual windowed segments, which is not the case for a continuously changing propagating wavelet. Enhanced resolution of nonstationary data using a molecular Gabor transform was described by *Wang et al. (2013)*.

Mallat and Zhang (1993) developed a matching pursuit approach to estimate sparse signals using time-frequency dictionaries. More recently matching and basis pursuit have been applied by a number of researchers for stationary and non-stationary time-series. For example, *Chai et al. (2014)* describe a basis pursuit inversion for nonstationary seismic data using frequencies within the seismic bandwidth and a cost function of mixed l_1 and l_2 norms without prior inverse Q filtering. *Zhang and Castagna (2011)* presented a basis pursuit inversion using a dictionary of reflectivity patterns. In addition to sparse-spike inversions, they developed inversions based on sparse-layer inversions that could be used to model thin beds and potentially provide improved resolution of fine layering.

Wang (2007) performed a matching pursuit for seismic trace decomposition. For increased stability *Wang (2010)* described a multi-channel matching pursuit approach for trace decomposition with optimal correlation between nearby seismic traces. *Lari and Gholami (2019)* investigated multichannel non-stationary blind deconvolution using a non-stationary block convolutional model and a variational approach in which the wavelets are allowed to change in both the vertical and horizontal directions.

In this study, we investigate a matching pursuit type of approach using a continuous non-stationary iterative time-domain deconvolution (CNS-ITD), where the propagating seismic wavelet is allowed to vary along the seismic trace. CNS-ITD was initially developed based on earlier studies by *Kikuchi and Kanamori (1982)* for the inversion of complex body-waves and *Ligorría and Ammon (1999)* for the estimation of seismic receiver functions, where the work of *Kikuchi and Kanamori (1982)* predates that of *Mallat and Zhang (1993)* on matching pursuit. However, instead of using a dictionary of functions for the sparse inversion, here the propagating wavelets for the CSN-ITD are first estimated in several overlapping Gabor windows of the data using a statistical approach.

Although the propagating wavelets could be used to estimate attenuation or scattering, here these are utilized to increase the resolution of the deconvolved data. Matrix-vector

operations in the time-domain are performed by interpolating in an efficient manner a small number of columns of the wavelet matrix for the sparse iterative estimation of the largest reflectivities. In this way, the method is less sensitive to variations of the small amplitudes in the time series in contrast to frequency-domain approaches. The iteration process is stopped when a minimum root mean square (*RMS*) residual or a maximum number of iterations is reached. We then convolve the results with a higher frequency wavelet in order to make the results more stationary in time and to increase the resolution of the data. We first apply CNS-ITD to synthetic data with a time-varying attenuation, where the method successfully identified the largest reflectors in the data. We then apply CNS-ITD to two observed shallow seismic datasets where improved resolution was obtained.

2. INITIAL OVERVIEW

Seismic data are often described by a convolutional model of the Earth's reflectivity with a seismic wavelet as

$$y(t) = s(t) * r(t) = \int_{-\infty}^{\infty} s(t-\tau) r(\tau)\, d\tau\,, \tag{1}$$

where $*$ is the convolution operator, $y(t)$ is the seismic trace, $s(t)$ is the seismic wavelet, and $r(t)$ is the reflectivity. Seismic deconvolution can then be used to remove the effects of the seismic wavelet and to estimate the reflectivity corresponding to a layered Earth. Performing seismic deconvolution, however, often has two unknown functions, the seismic wavelet and the reflectivity series, and only one known function, the seismic trace. However, if the reflectivity is statistically white, any variability of the power spectrum of the seismic trace can be attributed to the seismic wavelet (*Webster, 1978*; *Yilmaz, 2001*). Another assumption is that the casual seismic wavelet has minimum phase, and this enables the calculation of the seismic wavelet's phase spectrum from the power spectrum. When this is not the case, other techniques can be applied (*Webster, 1978*; *Robinson and Osman, 1996*). However, here we will emphasize either causal or pre-processed zero phase wavelets.

In conventional seismic processing, the seismic wavelet is assumed to be invariant along the seismic trace, and the amplitude and shape of the seismic wavelet do not change as it propagates in the subsurface. In practice, however, the seismic wavelet can change due to seismic attenuation and scattering effects in the Earth. Thus, the conventional convolutional model is often insufficient in representing non-stationary effects on the seismic data. The stationary convolution model can, however, be extended to the non-stationary case using more general matrix-vector operations (*Margrave, 1998*; *Margrave and Lamoureux, 2019*).

Equation (1) can be implemented numerically as a matrix multiplication by assigning the seismic trace (t) and the reflectivity $r(t)$ as column vectors, $\boldsymbol{y}$ and $\boldsymbol{r}$ respectively, and by constructing an $\mathbf{S}$ matrix which includes the seismic wavelet as

$$\boldsymbol{y} = \mathbf{S}\boldsymbol{r}\,. \tag{2}$$

For the stationary case, **S** is a Toeplitz matrix formed by progressively time-shifted versions of the same seismic wavelet (t) along the columns of **S**. The matrix multiplication in Eq. (2) involves multiplying each sample of the reflectivity series by the columns of the **S** matrix. Superpositions of the scaled and delayed seismic wavelets are then produced, and this represents the convolution process.

When the seismic wavelet changes in time, for example when attenuation is present, the matrix-vector multiplication above can still be applied, however in this case the **S** matrix no longer has Toeplitz symmetry (*Margrave, 1998*; *Margrave and Lamoureux, 2019*). The columns of the **S** matrix represent the propagating seismic wavelet changing in time. The non-stationary character of the seismic trace may be caused not only by attenuation but also by other effects, such as seismic scattering, that can alter the propagating seismic wavelet resulting in an amplitude reduction and a loss of frequencies.

3. METHOD

Iterative time-domain deconvolution (ITD) was developed by *Kikuchi and Kanamori (1982)* for the inversion of complex body-waves, and *Ligorría and Ammon (1999)* applied this to the estimation of seismic receiver functions for crustal structure. The ITD approach can also be used to iteratively reconstruct the seismic reflectivity series. ITD is a type of matching pursuit but was developed prior to the work of *Mallat and Zhang (1993)*. To implement this, the seismic wavelet and the seismic trace are first cross-correlated, and the maximum is found to locate the strongest reflectivities. These estimates of the reflectivity are then convolved with the seismic wavelet to obtain a predicted output trace, and the result is subtracted from the seismic trace to form a residual trace. This process is iterated until the mean square error (*MSE*) between the observed and predicted trace has sufficiently decreased. This is illustrated in Fig. 1 that shows a synthetic seismic trace formed by the convolution of a seismic wavelet with a reflectivity series including 4 reflectors. One percent Gaussian noise has also been added to the seismic trace. The estimated reflectivity at the final iteration is shown in Fig. 1 and is a good match with the true reflectivity.

The ITD approach can also be viewed as a matching pursuit type of algorithm for a seismic wavelet across the seismic trace. When there is a match, the algorithm removes the seismic wavelet and puts a spike at that location. Like other deconvolution methods, the ITD method is typically designed for stationary signals. However, by modifying the algorithm, it can also be applied to remove non-stationary propagating seismic wavelets (*Morozov et al., 2018*). The reflectivity series can then be iteratively updated from non-stationary template matching. The ITD approach has several desirable characteristics, which include finding the largest reflectivities first in a time window, and also providing control over when to stop adding smaller peaks to the inversion, and can result in less sensitivity to lower amplitude noise as compared to frequency-domain deconvolution methods.

The reflectivity series can be iteratively found as

$$\boldsymbol{y}^{i+1} = \boldsymbol{y}^{i} - r_i * \left(\mathbf{S}_{\text{column } j} \right), \tag{3}$$

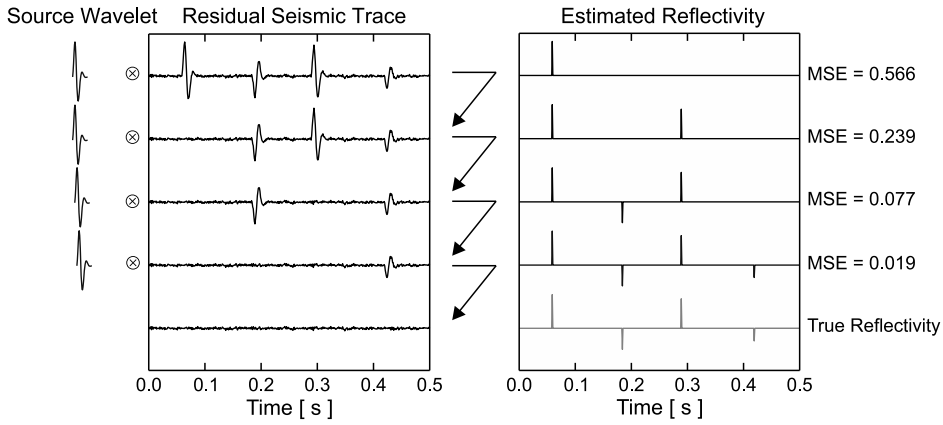

Fig. 1. Illustration of iterative time-domain deconvolution for the stationary case where 1% random noise has been added to the seismic trace. At each iteration, the reflectivity is determined by finding the maximum of the cross-correlation, denoted by ⊗, with the seismic wavelet shown on the left and the residual seismic trace is formed. To the right the iteratively updated reflectivity is shown with the true reflectivity displayed at the bottom. The reduction of the mean square error (*MSE*) is shown on the far right for each iteration. The final output of the iterative time-domain deconvolution is seen to be a good match to the true reflectivity (gray).

where * denotes convolution, i is the iteration number, $\mathbf{S}_{\text{column } j}$ is the j-th column of the **S** matrix, and the reflection coefficient r_i is then found by

$$r_i = \frac{\left(\mathbf{S}_{\text{column } j}\right)^{\mathrm{T}} \boldsymbol{y}^i}{\left(\mathbf{S}_{\text{column } j}\right)^{\mathrm{T}} \left(\mathbf{S}_{\text{column } j}\right)}, \quad i = 1, 2, 3, \ldots, N. \tag{4}$$

The largest peaks in the dot product $\left(\mathbf{S}_{\text{column } j}\right)^{\mathrm{T}} \boldsymbol{y}^i$ can be used to determine the sequential values for the reflection coefficient r_i at the i-th iteration. The location of the peak value of this multiplication gives the arrival time for this event and the result is then normalized by the dot product of the j-th column of **S** with itself to obtain an estimate of the reflection coefficient r_i at the i-th iteration. After finding the first reflectivity coefficient and its location, we convolve it with the j-th column of the **S**, and subtract this from the seismic trace to find $\boldsymbol{y}^{i+1}$ for the next iteration.

The construction of the **S** matrix, and therefore knowledge of the seismic wavelet is required to implement the algorithm given above. However, once the seismic wavelets have been estimated, specific columns of **S** can be efficiently obtained by interpolation at each iteration. There are a number of ways of estimating the seismic wavelet. Here we use an approach that assumes that the reflectivity is statistically white, and the power spectrum of the seismic wavelet can then be estimated from the tapered autocorrelation of the seismic trace. This can be applied either to the entire trace for the stationary case, or in overlapping Gabor windows of the data in the non-stationary case.

Figure 2 illustrates the wavelet estimation process for the stationary case. First, using the reflectivity series shown in Fig. 2a, a synthetic trace in Fig. 2b is formed by convolving the reflectivity series with a seismic wavelet. The autocorrelation of the seismic trace is found, and this is then windowed around zero lag as in Fig. 2c. Here, a shorter window length produces a smoother power spectrum, however, this may lack the full characteristics of the seismic wavelet. Thus, an appropriate window length needs to be chosen. For an impulsive source, the second zero-crossing of the autocorrelogram can sometimes be used to produce a good estimation of seismic wavelet as in predictive deconvolution (*Yilmaz, 2001*). Figure 2d shows the resulting zero phase windowed autocorrelation. To obtain a casual wavelet, a minimum phase can be added to obtain a minimum phase seismic wavelet.

If the seismic wavelet is minimum phase, then its phase spectrum can be uniquely obtained from its amplitude spectrum. The minimum phase estimate is obtained by taking the Hilbert transform of the log amplitude spectrum (*Webster, 1978*). Figure 2e shows the true minimum phase seismic wavelet for the synthetics (grey dashed) and the estimated seismic wavelet (black).

In the case of a stationary seismic wavelet, the **S** matrix can be built using only one estimated seismic wavelet, and the auto- and cross-correlations can be performed using the fast Fourier transform, FFT. If the seismic wavelet is not stationary, non-stationary deconvolution requires different propagating seismic wavelets at different times to compensate for the changing characteristics of the wavelet along the seismic trace. One way to construct a non-stationary **S** matrix is to move a properly chosen time window across the seismic trace one time sample at a time, and estimating the propagating seismic wavelet in each time window. These can then be assigned to the related columns of **S**. Although this provides a way for obtaining the changing seismic wavelet continuously, it is not an efficient time-domain implementation, especially for long seismic traces. Instead, here we initially divide the trace into a smaller number of overlapping windows for the estimation of the propagating wavelet in different time windows (*Margrave and Lamoureux, 2001, 2019*; *Grossman et al., 2002*). This can be written as

$$y(t) = \sum_{k=1}^{M} y_k(t, t_c) = \sum_{k=1}^{M} \Omega_k(t, t_c)\, y(t), \tag{5}$$

where $y_k(t, t_c)$ is the windowed segment of the seismic trace, Ω_k is the window function and M is the number of windows. The windowed segments of the seismic trace can be thought of as resulting from the convolution of propagating seismic wavelets and local reflectivity in that window, and this can be represented as

$$y_k(t, t_c) \approx s(t, t_c) * r(t, t_c), \tag{6}$$

where $s(t, t_c)$ is the locally stationary seismic wavelet in the window centered at t_c and $r(t, t_c)$ is the local reflectivity in that window. The seismic wavelet, (t, t_c), can then be estimated in each window and this carries information about the local propagating wavelet.

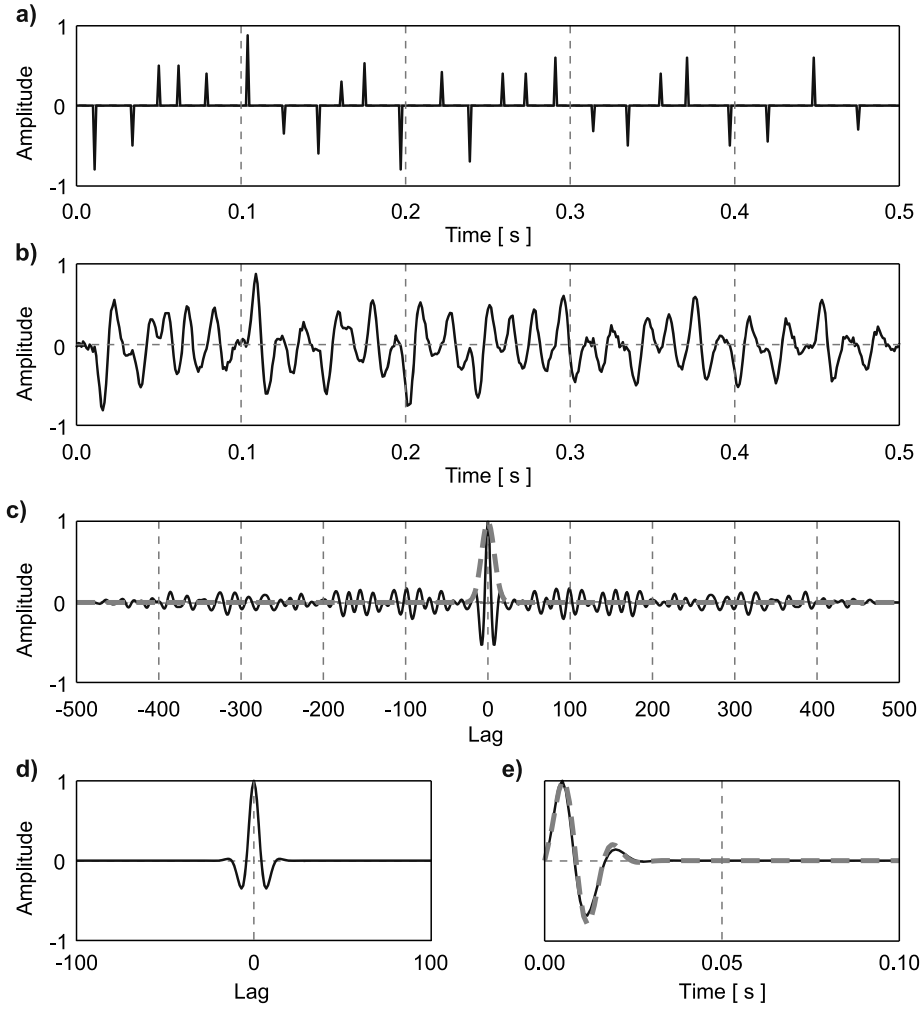

Fig. 2. Illustration of the wavelet estimation process in the stationary case. **a)** The reflectivity series, and **b)** the seismic trace including where 1% Gaussian noise has also been added; **c)** the autocorrelation of the seismic trace. A Gaussian window is applied (dashed gray line) to the autocorrelation of the trace around the zero lag. **d)** The windowed autocorrelation of the seismic trace, and **e)** a minimum phase version of the estimated wavelet (black), and the true seismic wavelet (gray dashed) which for this example is also minimum phase.

This approach assumes that the individual windowed segments of the seismic trace are locally stationary, and a stationary deconvolution can be applied within each window. For continuously varying propagating wavelets, such as from seismic attenuation or scattering, locally stationary deconvolution would be less accurate unless the windows lengths are chosen to be small enough. However, the matrix-vector version of the non-stationary

convolution model can still be applied. To perform non-stationary deconvolution for a continuously varying seismic wavelet, the propagating seismic wavelets can be interpolated in time so as to change smoothly along the seismic trace. Once the propagating wavelets are estimated in each window, these can then be assigned to corresponding columns of the **S** matrix at the center times of the windows. In this way, only a small number of columns of the **S** matrix are estimated. Other columns of the **S** matrix can then be found in an efficient manner by interpolation within the iterative process from a smaller number of estimated propagating wavelets. Here, we determine the corresponding columns of the **S** matrix from the peaks of the envelope of the seismic trace, instead of the peaks of the cross-correlation.

The distinction between the approach followed here and that of *Margrave et al. (2011)* and *Margrave and Lamoureux (2019)* in the frequency-domain, and *Morozov et al. (2018)* using the iterative time-domain approach is that the propagating wavelet is allowed to vary continuously along the seismic trace. The individual columns of the wavelet matrix can be quickly determined by interpolation within the sparse iterative time-domain estimation for the largest reflecitivities in the time series. We refer to this as continuous non-stationary iterative time-domain deconvolution (CNS-ITD).

3.1. Synthetic example

To illustrate the CNS-ITD process, a synthetic example is used to evaluate our approach in both the stationary and non-stationary cases. The seismic wavelets are estimated in sub-windows and used to construct the columns of the **S** matrix corresponding to the centers of each window. In the stationary case, the FFT can be used to obtain the cross- and auto-correlations for the ITD approach. Here we apply the CNS-ITD approach with a matrix-vector approach.

For the first example, the seismic wavelet is assumed to be stationary along the seismic trace, and all the columns of the **S** matrix can be filled with one estimate of the seismic wavelet estimated from the entire seismic trace. Even though we can construct the full **S** matrix, it does not mean that in the iteration process all the columns will be used for estimating the reflectivity series. At each iteration of the CNS-ITD process, only one column of the **S** matrix is used and this significantly reduces the computation time compared to full matrix-vector multiplications. We estimate the specific columns of the **S** matrix by the maximum peaks of the envelope of the seismic trace. In the case of a centered zero-phase wavelet, the location of the reflectivities and the peak of the envelope in the seismic trace are at the same location. For a casual seismic wavelet, however, there is a time shift between these two times. To address this, we use the difference between the beginning time and peak of the envelope of the estimated casual seismic wavelet as a time shift to correctly locate the reflectivity at the appropriate times as

$$\Delta t_i = t_i^e - t^0 , \tag{7}$$

where t^0 is the initial time and t_i^e is the time of the envelope peak of the estimated seismic wavelet. Once this time shift is found, the appropriate column of **S** can be determined. For the stationary case, the time shift Δt_i is a constant value along the entire seismic trace

since the seismic wavelet is time-invariant. For the non-stationary case, where the propagating seismic wavelet is changing in time, the time shift also changes along the seismic trace. For a zero phase wavelet, the time shift would be zero.

Although a local stationary deconvolution could be applied for each windowed segment of the seismic trace, it is not ideal since it does not allow for a continuously varying seismic wavelet. For seismic attenuation and scattering losses, the seismic wavelet evolves continuously as it propagates even within windowed segments of the seismic trace, and this can be achieved by interpolation of the propagating seismic wavelets along the seismic trace.

Figure 3 illustrates the approach for the stationary case, where for each iteration, the maximum peaks of the envelope of the full seismic trace are sequentially found. The corresponding columns of the **S** matrix are chosen from the estimated seismic wavelet. Using the location of the maximum of the envelope of the seismic wavelet, Δt_i can be estimated and the columns of the **S** matrix found. Equation (4) is then applied to find the corresponding reflectivity shown on the right on Fig. 3 for each iteration. The estimated reflectivities at each iteration are then adaptively removed from the seismic trace by applying Eq.(3). Since this is an iterative process, we can terminate the process either by specifying the total number of iterations or by the reduction in the *MSE* between the predicted trace and the observed seismic trace. After the iteration process shown in Fig. 3, all the reflectivities have been successfully recovered from the seismic trace, and *MSE* is close to the noise level added to the synthetic trace.

As noted previously, for the stationary case or by assuming stationarity in windows of the data, the reflectivity can be determined by calculating cross- and auto-correlations, which can be estimated using the FFT. However, in the CNS-ITD only a sparse number of columns are required and these can be cost effectively determined by interpolation of selective columns of the wavelet matrix within the sparse iterative deconvolution. In the context of iterative time-domain deconvolution, we are only estimating the largest reflectivities of the full seismic trace, and this helps to reduce the costs of the matrix-vector operations.

To deal with the non-stationary case, the propagating seismic wavelets along the seismic trace are first estimated for windowed segments of the seismic trace. The length of the window is an important parameter that needs to be carefully determined. In practice, the window length should be longer than that of propagating seismic wavelet in order to get a good estimate. Also, the distance between the window centers should be small enough so that changes in the propagating wavelet can be estimated, particularly if the seismic attenuation varies rapidly. The propagating seismic wavelets are then estimated from the localized windowed segments of the seismic trace in a data-driven way, and not assuming a simple attenuation model. The propagating seismic wavelets can then be interpolated as required for the iterative estimation to find the largest reflectivities.

Spectrograms are very useful in analyzing signals whose frequency content is changing in time. An example of the spectrogram of a synthetic non-stationary trace resulting from attenuation is shown in Fig. 4. The amplitude spectrum is shown on the left for the non-stationary seismic trace shown at the bottom. It can be seen both from the seismic trace and spectrogram that the bandwidth of frequencies is being reduced by the non-stationary filtering. In particular, frequencies greater than 75 Hz are attenuated for

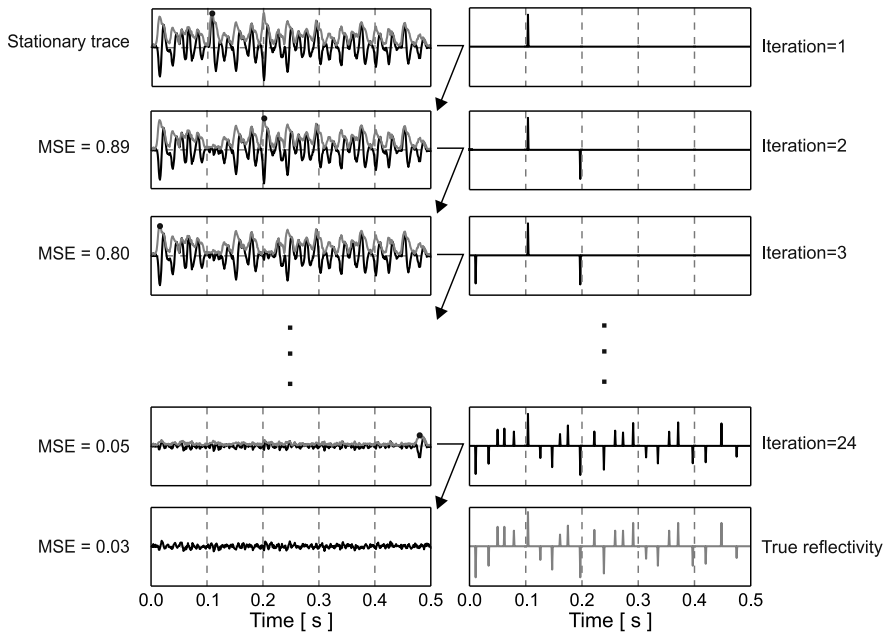

Fig. 3. Iterative time domain deconvolution for the stationary case. The synthetic trace is shown on the top left and 1% Gaussian random noise has been added. At each iteration, the location of the maximum peak of the envelope of the seismic trace is found which is denoted by black dot, and the corresponding propagating wavelet is chosen from the column of the **S** accounting for the time shift Δt described in Eq. (7). Using the seismic trace and the propagating wavelet, Eq. (4) is applied to estimate the reflectivity shown on the right. The estimated reflectivity is then subtracted from the seismic trace for the next iteration using Eq. (3). After a sufficient number of iterations, all the reflectivities are recovered from the seismic trace. The true reflectivity is shown on the bottom right. *MSE* – mean square error.

later times, along with a loss of amplitude resulting, and this leads to a lower resolution of the seismic data for greater times.

Using window partitions of the seismic trace, estimates of the propagating seismic wavelets can be made in each of the windows in order to construct selected columns of the **S** matrix. Figure 5a,b depict the windows and estimated propagating wavelets at the center of each window. As can be seen, the estimated seismic wavelets are time-varying, losing amplitude and spectral content with time as shown in the spectrogram in Fig. 4. Using the center times of the windows, these are assigned to the columns of the **S** matrix, which are shown in Fig. 5c. These can then be interpolated to determine selected columns of the **S** matrix where the maximum values of the envelope of the seismic trace occur, including the time shift given in Eq. (7). Continuous non-stationary iterative time-domain deconvolution (CNS-ITD) can then be performed to find the largest reflectivities in time along the seismic trace. As noted previously, an advantage of this approach is that it allows one to find any desired number of the strongest reflectivities, leading to a sparse deconvolution of the seismic trace.

Figure 6 illustrates the CNS-ITD of the seismic trace shown in Fig. 5a where 1% Gaussian random noise has been added. The addition of further random noise can affect the estimation of the smaller reflectivities, but less so for the sparse larger reflectivities. We used a different number of iterations as shown in Fig. 6b to estimate the full reflectivity series. For iteration 5, this gives five reflectivity estimates along the seismic trace. The residual traces in Fig. 6a are then found by iteratively subtracting the predicted traces at each iteration. The residuals become smaller with an increasing number of iterations, and the *MSE* is reduced shown on the left. Figure 5d shows the estimated columns of the **S** matrix determined as part of the iteration process. Since we are performing a sparse iterative inversion for the larger reflectivites, the fewer number of columns utilized in the **S** matrix makes the time-domain implementation cost effective. We used both linear and spline interpolation, but the differences were not significant for the cases given here and the results for a spline interpolation are used.

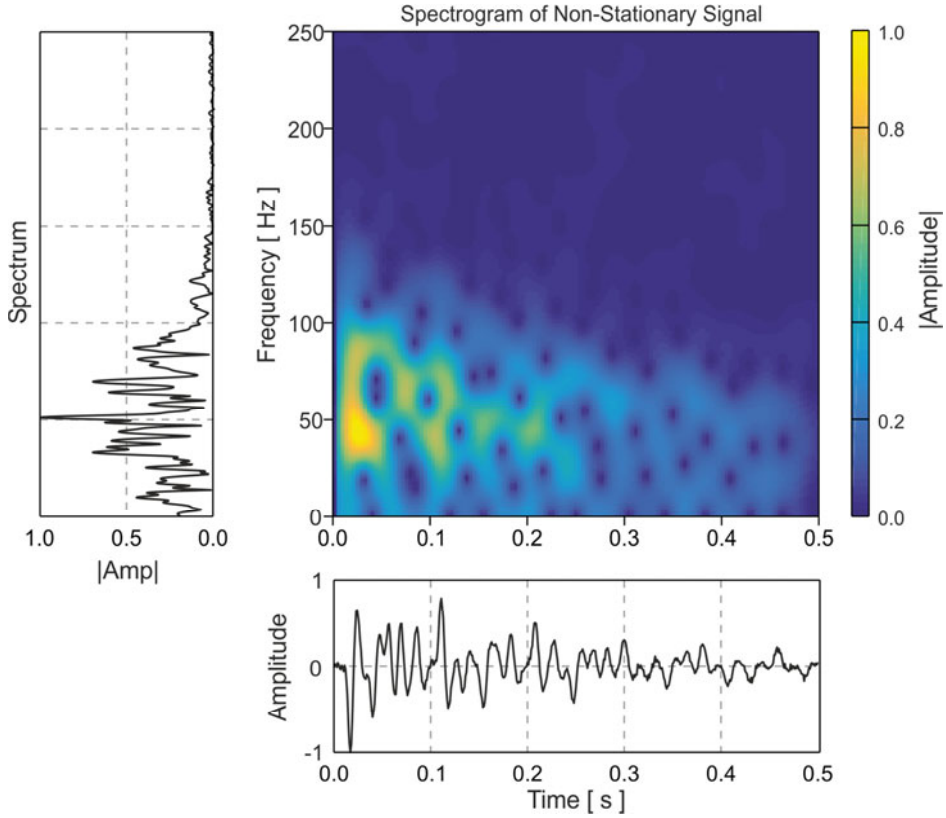

Fig. 4. The spectrogram of a non-stationary seismic trace. The Fourier amplitude spectrum is shown on the left for the non-stationary seismic trace shown at the bottom. 1% Gaussian random noise has also been added to the non-stationary seismic trace. It can be seen that frequencies greater than 75 Hz are being reduced for increasing time for this example.

After 30 iterations, the full reflectivity series has been recovered. Note, however, that several smaller additional reflectivity values have also been found. Since the estimation of the propagating wavelets includes some errors in terms of waveform and amplitude, some residuals will be present between the predicted and true reflectivities resulting from this. If we further increase the iteration number, the ITD approach will treat the remaining

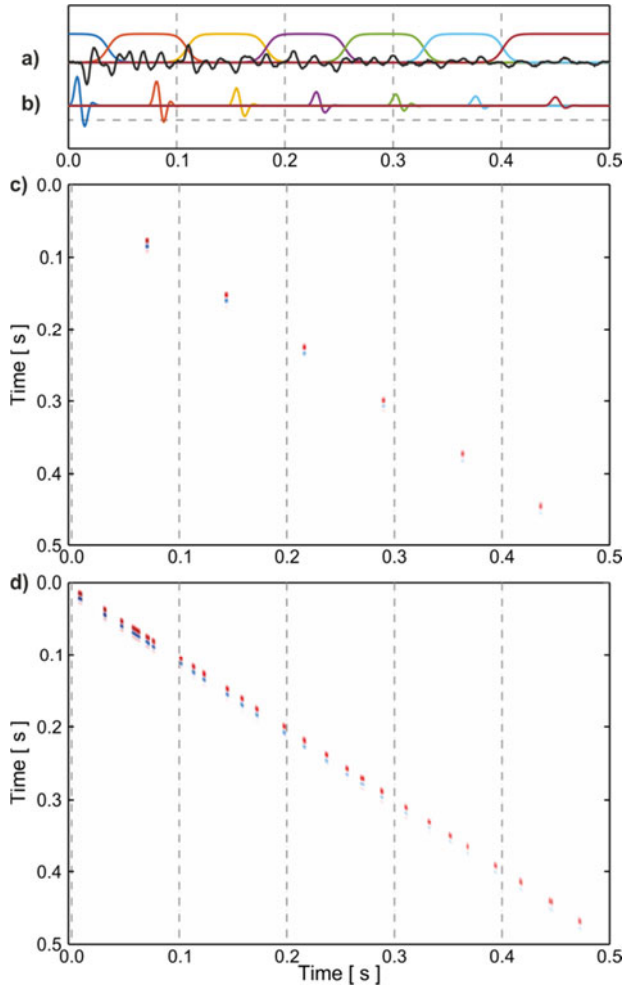

Fig. 5. **a)** Non-stationary seismic trace along with window functions used to window the seismic trace; **b)** the estimated propagating seismic wavelets for each of the windows. **c)** The columns of the **S** matrix, where the propagating wavelets are assigned at the centers of the window functions shown in a). These are displayed by short vertical pulses. The dashed lines are shown for reference at every 0.1 seconds. **d)** The columns of the **S** matrix resulting from the sparse CNS-ITD inversion. These are again shown by short vertical pulses, and are obtained by interpolation of the propagating wavelets shown in b). The dashed lines are shown for reference at every 0.1 seconds.

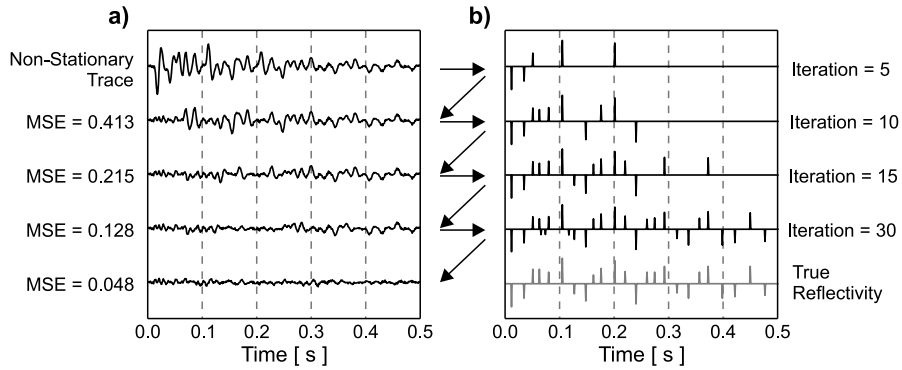

Fig. 6. Continuous non-stationary iterative time-domain deconvolution (CNS-ITD) is performed along the seismic trace shown in Fig. 5a) for different numbers of iterations. For iteration 5, five reflectivities are found along the seismic trace, and these are increased until all the reflectivities have been recovered. As the number of iterations is increased, the mean square error of the residual trace is decreased which can be seen in **a)**. When the number of iterations is increased, the CNS-ITD approach will try to recover more reflectivities in **b)** from the residuals shown in a).

residuals as signal and try to produce new reflectivities. However, since all the strongest reflectivities have been estimated and removed from the seismic trace, remaining reflectivities will be small. The estimated reflectivities can then be re-convolved with a stationary wavelet to construct a stationary and higher resolution seismic trace.

Since our approach iteratively estimates the largest reflectivities that are assumed to be sparse, the inclusion of small amounts of random noise does not affect the estimation of the largest reflectivities. This is appropriate for models that have either a white spectrum or a red-shifted spectrum for the larger reflectivities. This might result from blocky structures where the sparse larger reflectivities dominate. However for smaller more densely sampled reflectivities then false envelope peaks could result. Nonetheless, **s**mall artifact reflectivities can be avoided by limiting the MSE error between the observed and predicted seismic trace.

In general for more densely sampled but stronger reflectivities, then other approaches may be more appropriate. *Zheng et al. (2019)* investigated thin-bed layers in the BoHai oilfield resulting in a non-white, blue spectrum for the reflectivity. *Zhang and Castagna (2011)* performed sparse-layer reflectivity inversion instead of spare-spike inversions to better model thin layers. This could also be investigated here with a suitable dictionary of thin-layer responses, but for this study we have only inverted for sparse inversions for the strongest reflectivities with responses estimated in the individual Gabor windows assuming a white spectrum.

4. OBSERVED DATA APPLICATIONS

We apply the CNS-ITD approach to two observed shallow seismic datasets from *Baker (1999)*. The first dataset was collected in an alluvial valley of the Thames River, England in 1989 to image bedrock stratigraphy and examine the structure and geometry.

Figure 7a shows the observed zero offset stacked data from *Baker (1999)*. The horizontal axis in this figure is trace number and the spacing between the traces is 1.25 m. The vertical axis is two-way reflection time down to 0.25 s. The processing steps applied to the data by *Baker (1999)* were pre-processing (geometry definition, killing the noisy traces), filtering the ground roll and air wave, static corrections, velocity analysis and stacking. To increase the lateral coherence, we have also applied a small amount of frequency-wavenumber (*f-k*) filtering to enhance the continuity and coherence between traces (Fig. 7b).

The non-stationary character of the seismic traces can be seen from the spectrogram for trace 10 shown in Fig. 8 where the spectrogram amplitudes show a slight decrease in frequency with time. This frequency decrease in time is evident even with relatively small reflection travel-times due to the alluvial medium at the site that can result in higher attenuation (*Steeples, 2005*).

Before applying CNS-ITD to the seismic section, we perform it on a single trace in order to determine the window size and iteration number to be applied for each of the traces. Figure 9a shows trace 10 used for the spectrogram in Fig. 8 and the windows that were used for partitioning of the trace to estimate the propagating wavelet for different travel-times. Figure 9b shows the estimated propagating wavelets for each of the

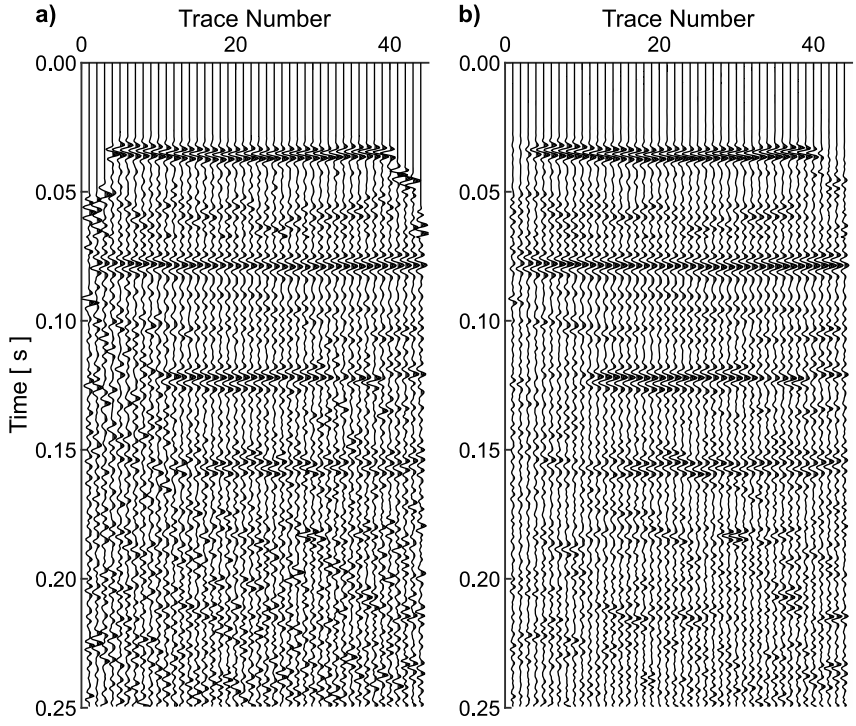

Fig. 7. **a)** Stacked section of the Thames River data obtained from *Baker (1999)*; **b)** the seismic stacked section with frequency-wavenumber filtering applied to slightly increase the lateral coherence.

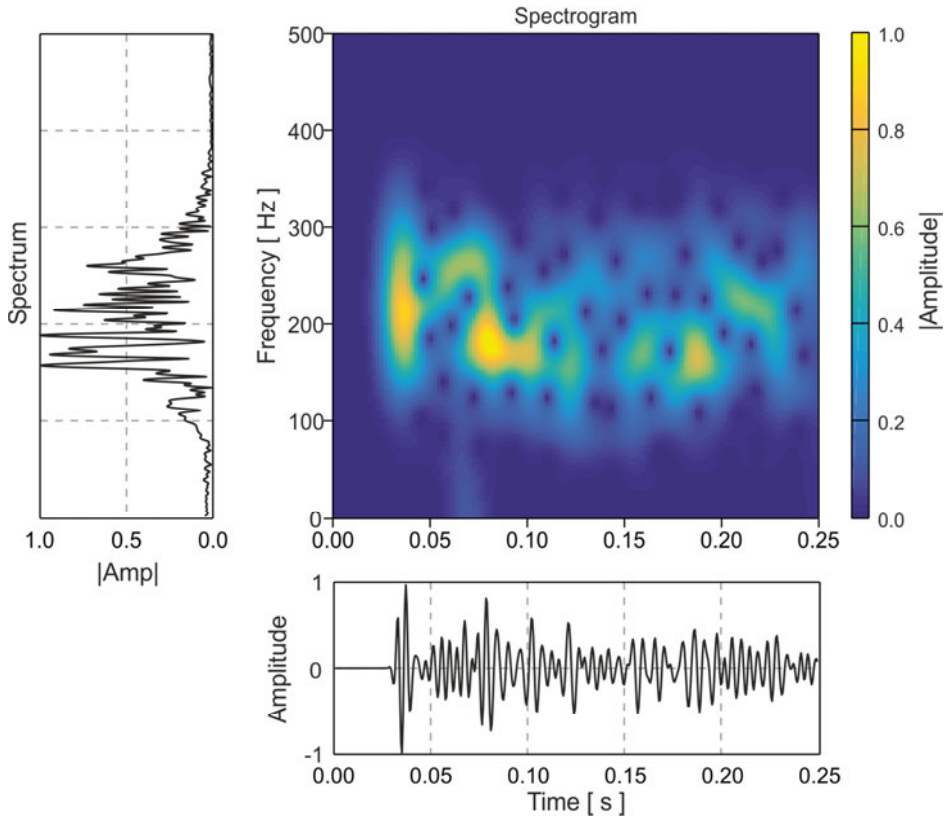

Fig. 8. Spectrogram of trace 10 from the stacked seismic section of the Thames River dataset shown in Fig. 7b). The non-stationary character of the seismic trace can be seen where the amplitudes of the spectrum show a decrease in frequency with time.

windows. In this case, since the data have been previously processed by *Baker (1999)*, we assume here that the non-stationary propagating seismic wavelets are zero phase and normalized to unit amplitude. These are then continuously interpolated along the trace iteratively within the CNS-ITD process to find the largest reflectivities.

We have used both the *MSE* and the total number of iterations as stopping criteria in the iteration process. Thus, if the maximum iteration number is reached or the *MSE* between observed and predicted traces is below a specific level, the process is terminated. Figure 9c shows trace 10 and residual traces calculated after application of CNS-ITD with different numbers of iterations given on the right side of the subplot, where iteration 10 signifies that ten iterations have been performed. The estimated spike diagrams for different numbers of iterations are shown in Fig. 9d. After ten iterations, only the strongest reflectivities have been determined. When the number of iterations is increased, a larger number of smaller reflectivities are obtained. When the iteration number has reached 60, the mean square error of the residual trace has been reduced to about 2%.

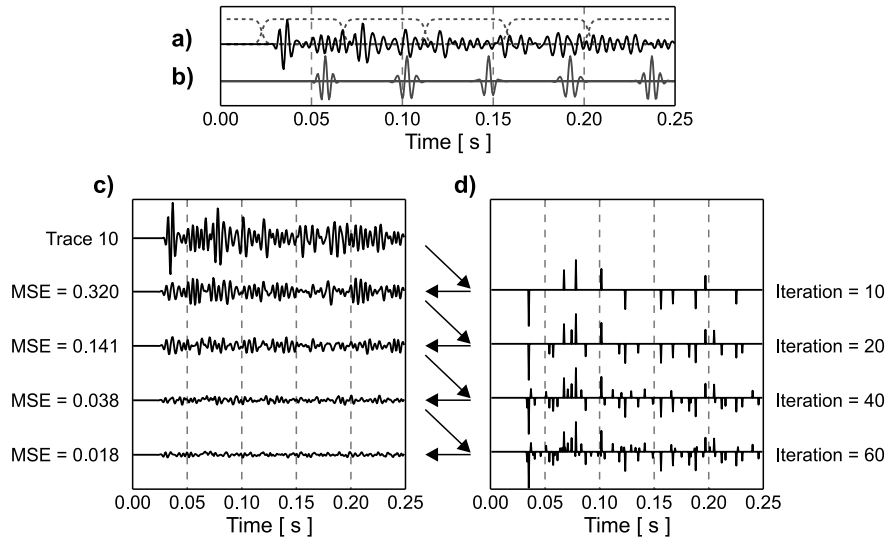

Fig. 9. An application of continuous non-stationary iterative time-domain deconvolution to trace 10 from seismic section shown in Fig. 7b). **a)** The seismic trace together with window functions, and **b)** the estimated propagating wavelets for each window. **c)** Trace 10 on the top and residual traces for different numbers of iterations; **d)** the spike diagram produced after performing ten iterations performed on the trace. Similarly, the results for different numbers of iterations for the residual traces and the mean square errors (*MSE*) are shown in c).

We then applied CNS-ITD to the full seismic section for the Thames River dataset. The output of the CNS-ITD are the deconvolved reflectivities similar to that shown in Fig. 9d for each trace. Seismic sections can then be obtained using a stationary Ricker wavelet with a particular dominant frequency. Figure 10a shows the deconvolution results of the CNS-ITD applied to the stacked seismic section in Fig. 7b. Figure 10b shows the results of the CNS-ITD after re-convolving with a stationary 250 Hz Ricker wavelet. To see the effect of the CNS-ITD on the seismic traces, we plot the spectrogram of the deconvolved trace 10 after CNS-ITD, and re-convolved with a stationary 250 Hz Ricker wavelet in Fig. 11. Comparing Figs 8 and 11, it can be seen that the frequency bandwidth of the trace has been improved with more uniform and higher frequency content.

The second observed dataset was located in Kansas to image whether there was a glacial meltwater channel cut into the bedrock, and then later covered by sediments (*Baker et al., 1998*; *Baker, 1999*). Similar processing steps applied to first dataset were also applied to the Kansas dataset by *Baker (1999)*. Figure 12a shows the original stacked section from *Baker (1999)* with some additional gain applied and Fig. 12b shows stacked section after *f-k* filter has been applied to increase lateral coherency. The horizontal axis in this figure is trace number and the spacing between the traces is 0.25 m. The vertical axis is two-way reflection time down to 0.2 s, with the near surface speeds this corresponds to a depth of approximately 40 m (*Baker, 1999*).

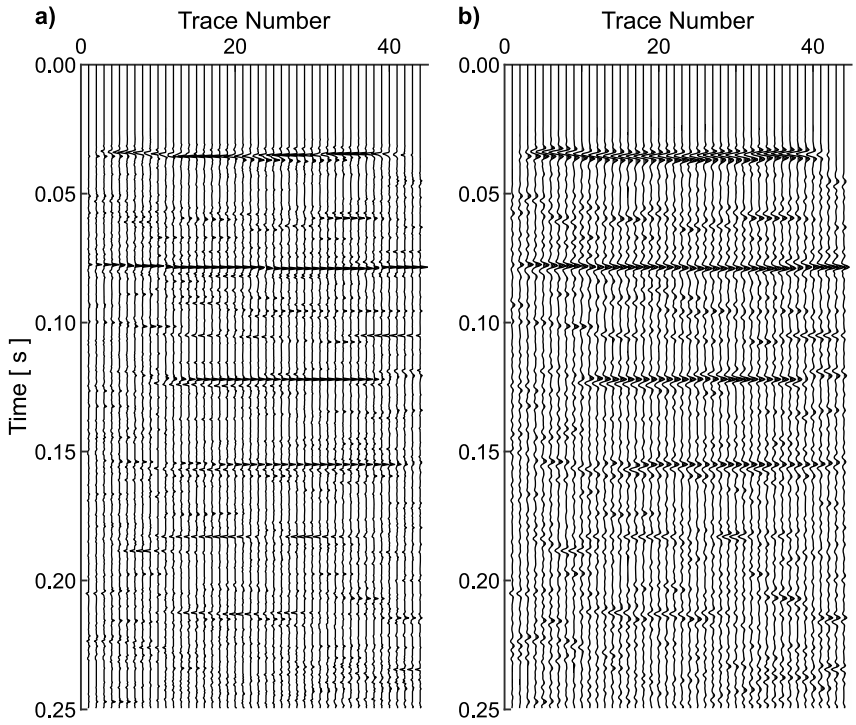

Fig. 10. a) The continuous nonstationary iterative time-domain deconvolution of the seismic section in Fig. 7b. **b)** The deconvolved results that have been re-convolved with a stationary 250 Hz Ricker wavelet, and an frequency-wavenumber filter has been applied to slightly increase lateral coherence.

We again selected a particular trace, here trace 75, to display a spectrogram of the frequency content with time, and this is shown in Fig. 13. As can be seen, the frequency content of the trace decreases with time. Figure 14 shows the CNS-ITD applied to this trace for different numbers of iterations. Figure 14a shows the seismic trace along with the window functions, and Fig. 14b shows the estimated propagating wavelets for each window. These are continuously interpolated within the CNS-ITD iterative process. Figure 14c shows the residual traces for different numbers of iterations along with the *MSE*. After 20 iterations the *MSE* has decreased to around one percent. The resulting deconvolved reflectivities are shown in Fig. 14d for different numbers of iterations. Since the data has been previously processed, the estimated propagating wavelets is assumed to be zero phase and normalized to unity.

We then performed the CNS-ITD on the full Kansas dataset. The resulting deconvolved reflectivities for each of the traces are then re-convolved with a stationary 100 Hz Ricker wavelet. An *f-k* filter was applied to slightly increase the lateral coherency. Figure 15a shows the deconvolution results of the CNS-ITD applied to the seismic section is Fig. 12b. Figure 15b shows the deconvolved results after re-convolving with

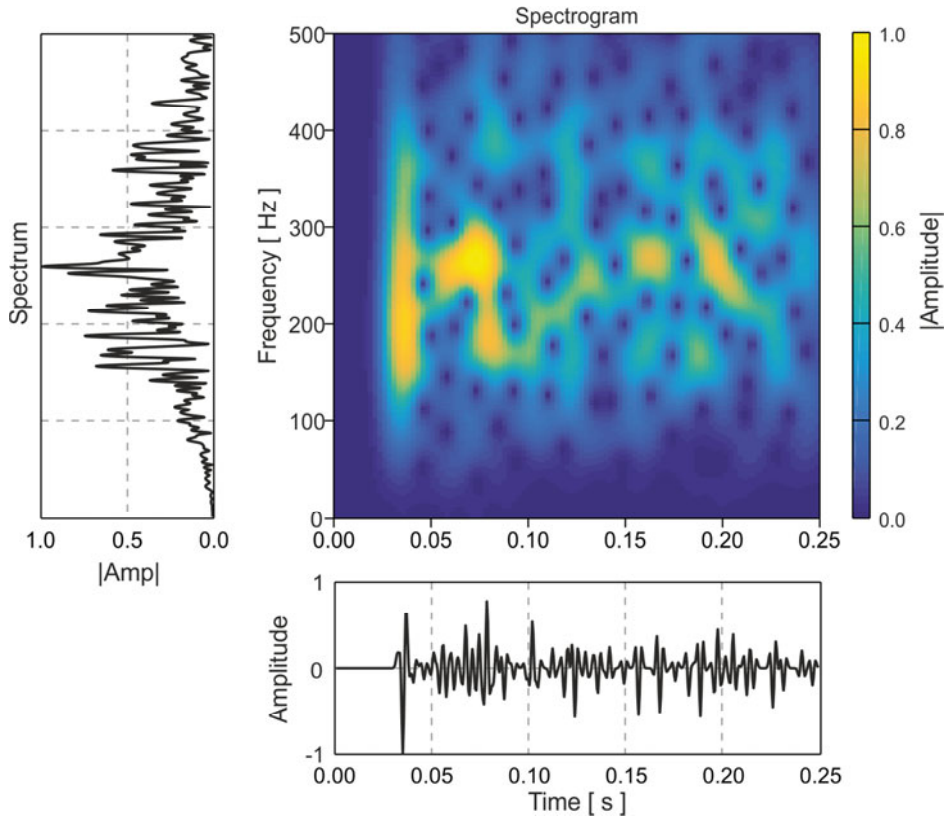

Fig. 11. Trace 10 from the seismic section shown in Fig. 7b after continuous nonstationary iterative time-domain deconvolution and re-convolved with a stationary 250 Hz Ricker wavelet. Comparing with Fig. 8, it can be seen from the seismic trace, the spectrum and the spectrogram that the frequency content has been increased and is more uniform with frequency after the deconvolution and re-convolution with a stationary 250 Hz Ricker wavelet.

a stationary 150 Hz Ricker wavelet. Some consolidation of reflectivities has resulted in part from the removal of the propagating wavelets within the iterative inversion process. There is also lateral variability along the profile and this could result in some of the deconvolved events being consolidated or a lost along the profile. However a majority of the largest reflectivities have been determined.

It can be seen that the resolution has been improved by applying CNS-ITD. This can be verified by the spectrogram of trace 75 after CNS-ITD re-convolved with a stationary 150 Hz Ricker wavelet, which is shown in Fig. 16. Although the overall frequencies of the spectrum have been increased, the lower and upper ranges of the spectrum are also affected by the re-convolution by the new stationary Ricker wavelet.

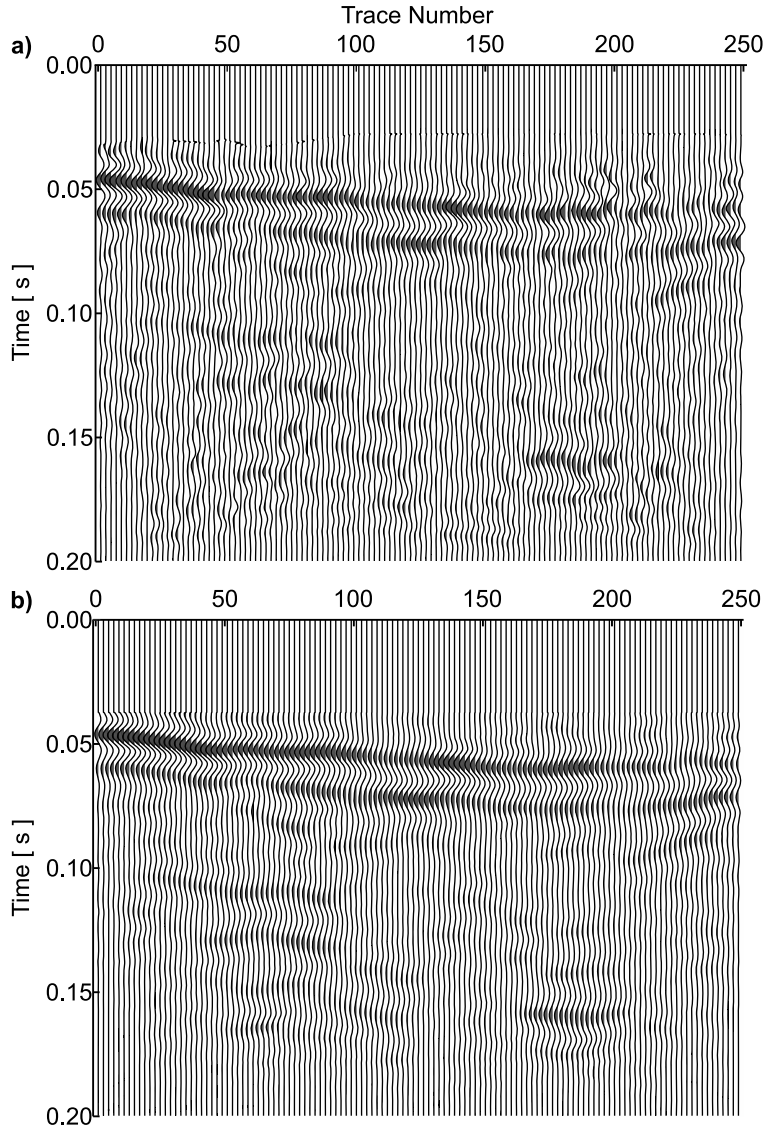

Fig. 12. **a)** Stacked seismic section of the Kansas dataset obtained from *Baker (1999)* with an additional gain applied, and **b)** the seismic stacked section with an frequency-wavenumber filter applied to increase lateral coherency.

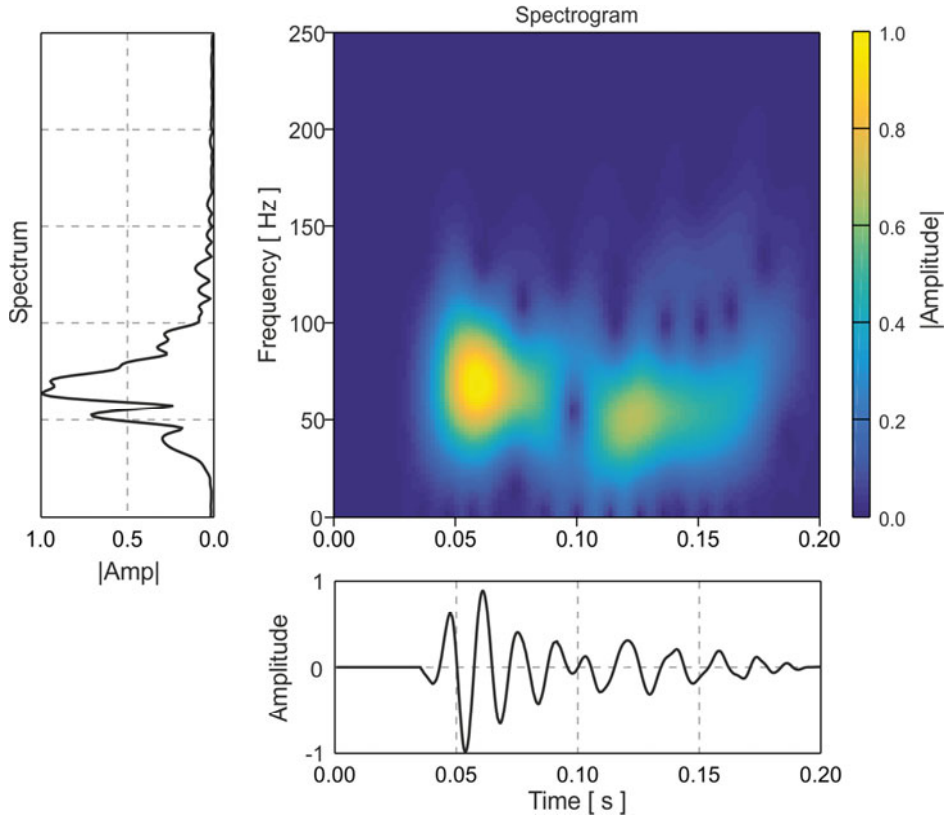

Fig. 13. Spectrogram of trace 75 from the stacked seismic section of Kansas dataset from *Baker (1999*) shown in Fig.12b. The non-stationary character of the seismic trace can be seen where the amplitudes of the spectrogram show a decrease in frequency with time.

5. CONCLUSIONS

In this study, a continuous non-stationary iterative time-domain deconvolution (CNS-ITD) has been investigated. This a type of matching pursuit algorithm, but was initially develop based on earlier studies by Kikuchi and Kanamori (1982) and Ligorria and Ammon (1999) in earthquake seismology. For CNS-ITD the propagating wavelets are first estimated in several overlapping Gabor windows of the data. Matrix-vector operations in the time-domain are then performed by estimating a small number of columns of the wavelet matrix by interpolation within a sparse iterative estimation for the largest reflectivities in the data. In this way, the method is less sensitive to variations of the smallest amplitudes in the time series in contrast to frequency-domain approaches. The iteration process is stopped when a minimum RMS residual or a maximum number of

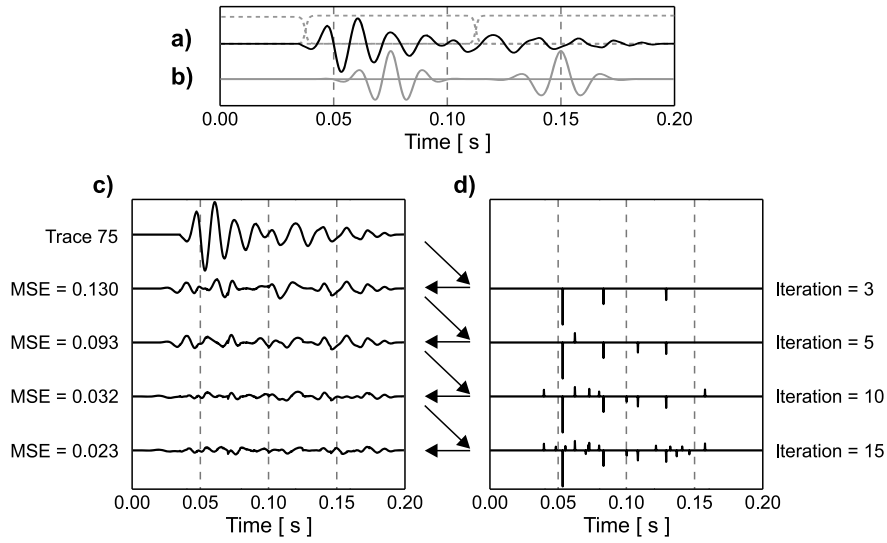

Fig. 14. An application of continuous non-stationary iterative time-domain deconvolution to trace 75 from the stacked section of Kansas dataset shown in Fig. 12b. **a)** The seismic trace together with window functions; **b)** the estimated propagating wavelets for each window. **c)** Trace 75 on the top and residual traces for different numbers of iterations; **d)** spike diagram produced after five iterations have been performed along the trace. Similarly, the results for different numbers of iterations are also shown in d), and the residual traces along with the mean square errors (*MSE*) are shown in c).

iterations is reached. The results are then convolved with a higher frequency wavelet in order to make the results stationary in time and to increase the resolution of the data. We tested CNS-ITD on both synthetic and observed data. For the synthetic data, we were able to successfully estimate the largest reflectivities in the data. Applying CNS-ITD to the observed data, higher frequencies were recovered and the resolution of the data was improved.

Acknowledgments: The authors thank the reviewers and Associate Editor for their constructive reviews, which substantially improved the manuscript. The first author thanks The General Directorate of State Hydraulic Works (DSI), Turkey for supporting his graduate studies at Purdue University. The study was partially supported by US National Science Foundation Grant 1839322. MATLAB software was used for the visualization and also several codes were modified from the CREWES MATLAB toolbox of the Consortium for Research in Elastic Wave Exploration Seismology, University of Calgary Calgary, Alberta, CANADA.

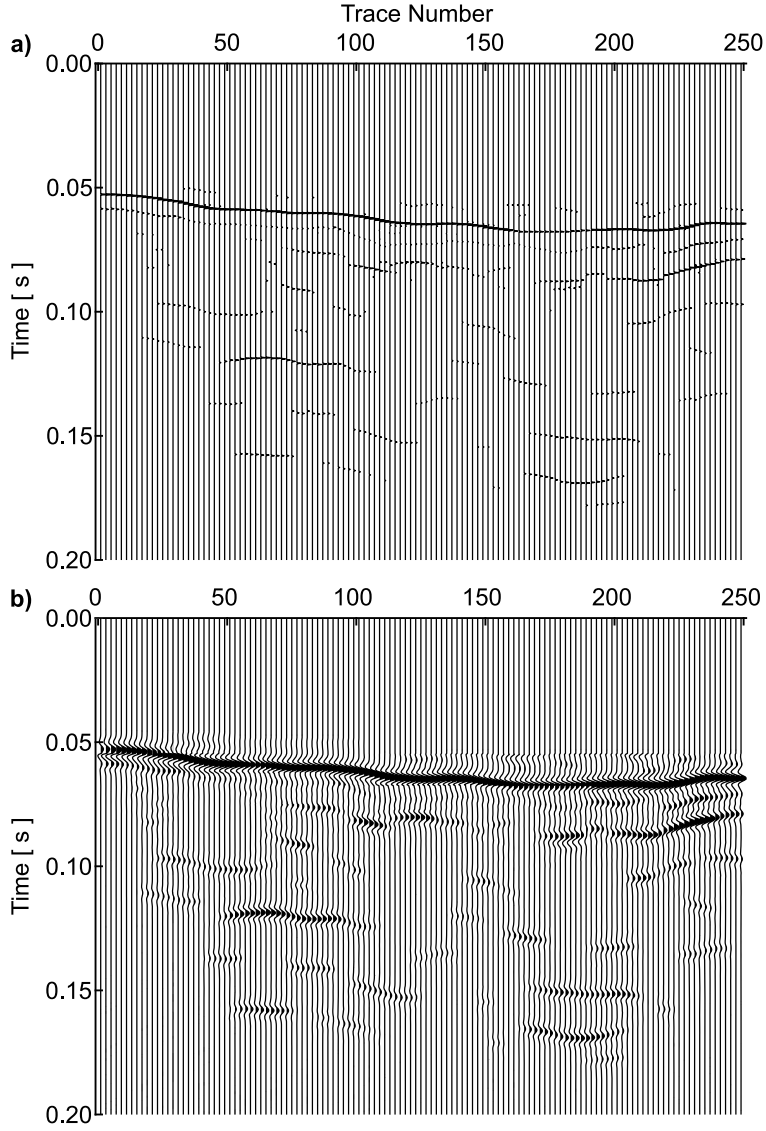

Fig. 15. **a)** Results of the continuous non-stationary iterative time-domain deconvolution of the seismic section in Fig. 12b. **b)** The deconvolved results, which have been re-convolved with a stationary 150 Hz Ricker wavelet. An frequency-wavenumber filter has also been applied slightly to increase lateral coherence.

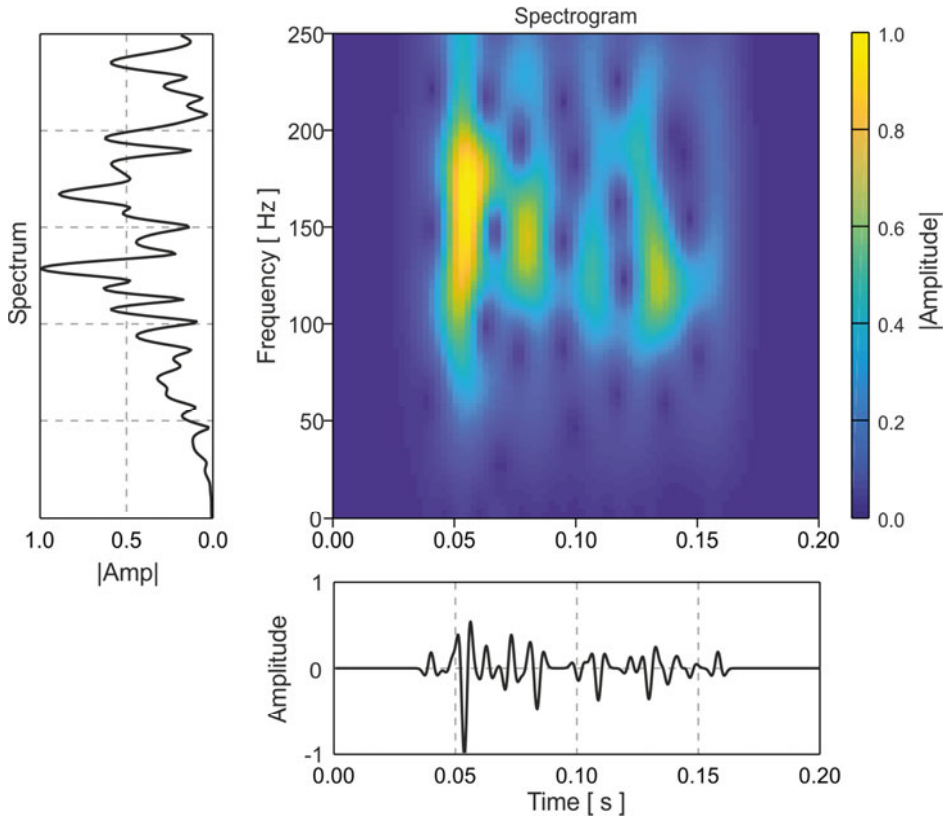

Fig. 16. Spectrogram of trace 75 from the stacked seismic section of the Kansas dataset from Fig. 12b after continuous non-stationary iterative time-domain deconvolution and re-convolved with a stationary 150 Hz Ricker wavelet.

References

Baker G.S., Steeples D.W. and Drake M., 1998. Muting the noise cone in near-surface reflection data: An example from southeastern Kansas. *Geophysics*, **63**, 1332–1338.

Baker G.S., 1999. *Processing Near-Surface Seismic-Reflection Data: A Primer*. Society of Exploration Geophysics, Tulsa, OK.

Chai X., Wang S., Yuan S., Zhao J., Sun L. and Wei X., 2014. Sparse reflectivity inversion for nonstationary seismic data. *Geophysics*, **79**, V93–V105.

Grossman J.P., Margrave G.F. and Lamoureux M.P., 2002. Constructing adaptive, nonuniform Gabor frames from partitions of unity. *CREWES Research Report*, **14**, 1–10, University of Calgary, Canada.

Hale D., 1981. An inverse-Q filter. *Stanford Exploration Project Report*, **26**, 133–158.

Kikuchi M. and Kanamori H., 1982. Inversion of complex body waves. *Bull. Seismol. Soc. Amer.*, **72**, 491–506.

Kjartansson E., 1979. Constant Q wave propagation and attenuation. *J. Geophys. Res.*, **84**, 4737–4748.

Lari H.H. and Gholami A., 2019. Nonstationary blind deconvolution of seismic records. *Geophysics*, **84**, V1–V9,

Ligorria J.P. and Ammon C.J., 1999. Iterative deconvolution and receiver-function estimation. *Bull. Seismol. Soc. Amer.*, **89**, 1395–1400.

Mallat S.G. and Zhang Z., 1993. Matching pursuits with time-frequency dictionaries. *IEEE Trans. Signal Process.*, **41**, 3397–3415.

Margrave G.F., 1998. Theory of nonstationary linear filtering in the Fourier domain with application to time variant filtering. *Geophysics*, **63**, 244–259.

Margrave G.F. and Lamoureux M.P., 2001. Gabor deconvolution. *CREWES Research Report*, **13**, 241–276, University of Calgary, Canada.

Margrave G.F. and Lamoureux M.P., 2019. *Numerical Methods of Exploration Seismology*. Cambridge University Press, Cambridge, U.K.

Margrave G.F., Gibson P.C., Grossman J.P., Henley D.C., Iliescu V. and Lamoureux M.P., 2005. The Gabor transform, pseudodifferential operators, and seismic deconvolution. *Integr. Comput.-Aided Eng.*, **12**, 43-55.

Margrave G.F., Lamoureux M.P. and Henley D.C., 2011. Gabor deconvolution: Estimating reflectivity by nonstationary deconvolution of seismic data. *Geophysics*, **76**, W15–W30.

Morozov I.B., Haiba M. and Deng W., 2018. Inverse attenuation filtering. *Geophysics*, **83**, V135–V147.

Robinson E.A. and Osman O.M. (Eds), 1996. *Deconvolution 2*. Geophysics Reprint Series, **17**, Society of Exploration Geophysics, Tulsa, OK.

Steeples D.W., 2005. Shallow seismic methods. In: Rubin Y. and Hubbard S.S. (Eds), *Hydrogeophysics*. Springer, Dordrecht, The Netherlands, 185–213.

Van der Baan M., 2012. Bandwidth enhancement: inverse Q filtering or time-varying Wiener deconvolution. *Geophysics*, **77**, V133–V142.

Wang L., Gao J., Zhao W. and Jiang X., 2013. Enhancing the resolution of nonstationary seismic data by molecular-Gabor transform. *Geophysics*, **78**, V31–V41.

Wang Y., 2006. Inverse Q-filter for seismic resolution enhancement. *Geophysics*, **71**, V51–V60.

Wang Y., 2007. Seismic time-frequency spectral decomposition by matching pursuit. *Geophysics*, **72**, V13–V20.

Wang Y., 2008. *Seismic Inverse Q Filtering*. Wiley-Blackwell, Malden, MA.

Wang Y., 2010. Multichannel matching pursuit for seismic trace decomposition. *Geophysics*, **75**, V61–V66.

Webster G.M. (Ed.), 1978. *Deconvolution*. Vols 1 and 2. Society of Exploration Geophysics, Tulsa, OK.

Yilmaz O., 2001. *Seismic Data Processing*. Vols 1 and 2. Society of Exploration Geophysics, Tulsa, OK.

Zhang R. and Castagna J., 2011. Seismic sparse-layer reflectivity inversion using basis pursuit decomposition. *Geophysics*, **76**, R147–R158.

Zheng J., Zhang Z., Sun J. and Liu G., 2019. The method of spectrum bluing based on spectrum inversion for improving seismic resolution. *SEG Technical Program Expanded Abstracts 2019*, 3464–3468, DOI: 10.1190/segam2019-3215862.1.